energy&fuels

Open Access

This article is licensed under CC-BY 4.0

pubs.acs.org/EF

Article

Utilization of Nanoparticles to Improve the Kinetics of CH_4 Gas Hydrates in Gas Storage Applications

Phakamile Ndlovu, Saeideh Babaee,* Paramespri Naidoo, and Kuveneshan Moodley

Cite This: *Energy Fuels* 2024, 38, 4480−4491

Read Online

ACCESS | Metrics & More | Article Recommendations | Supporting Information

ABSTRACT: Increasing energy demands have opened research channels into alternate areas to explore viable options for energy storage. This has led to investigations into the use of gas hydrate technology, specifically derived from methane gas, for diverse energy applications, such as gas storage and gas transportation. In this study, the kinetics of CH_4 hydrate formation in (0.1, 0.2, 0.5, 1.0, and 1.2 wt %) CuO and Al_2O_3 nanoparticles, graphene nanoplatelets, and ZnO microparticles in the presence of 0.05 wt % sodium dodecyl sulfate (SDS) were measured experimentally. The experimental measurements were conducted in a 52 cm^3 equilibrium cell at a pressure of 4.66 MPa and a temperature of 275.8 K. The kinetic parameters under investigation included the induction time, storage capacity, water conversion, rate of gas uptake, and gas consumption. Results show that the inclusion of nanoparticles in the experiments decreased the induction time from 18.4 min with deionized water to 1.0 min with 0.1 wt % CuO + 0.05 wt % SDS while the induction period increased to 20.7 min with 1.2 wt % ZnO + 0.05 wt % SDS microparticles. A maximum storage capacity of 28.5 (v/v) was obtained using 0.1 wt % CuO + 0.05 wt % SDS. The highest gas uptake rate recorded was 8.9×10^{-4} mol gasmol $water^{-1}$ min^{-1}, achieved with the combination of 0.5 wt % CuO + 0.05 wt % SDS. Overall, the parameters investigated in this study indicated a significant enhancement in the rate of hydrate formation with the inclusion of nanoparticles.

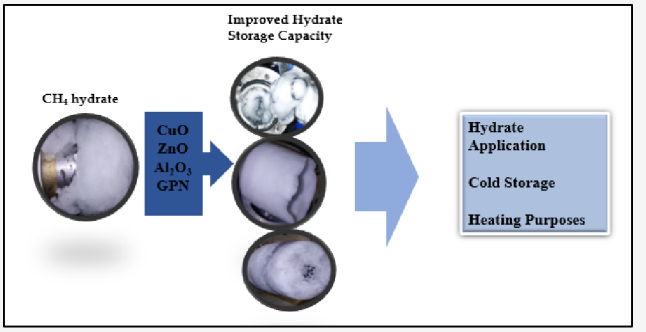

Downloaded via 165.73.48.38 on April 13, 2024 at 17:19:08 (UTC).
See https://pubs.acs.org/sharingguidelines for options on how to legitimately share published articles.

1. INTRODUCTION

Gas hydrates, or clathrates, are nonstoichiometric compounds comprising minute gas molecules like methane, carbon dioxide, and propane enclosed within a lattice of water molecules. Research has demonstrated that clathrates possess a significant storage capability, with 1 cm^3 of hydrate able to accommodate up to 150 m^3 of natural gas, surpassing the storage efficiency of compressed or liquid natural gas under secure conditions.[1−3] Due to its expandable storage volume, the gas hydrates have been utilized for gas separation with a lower energy pathway as compared to convection methods in the isolation of xenon from its trinary combinations with krypton and argon.[4] An examination of the practicality of employing gas hydrate for biogas storage, a sustainable energy source with a minimal environmental footprint, revealed that two economically viable methods can be employed to convert biogas into biomethane.[5] In addition, in a study on the natural gas hydrate formation at the temperature of 277 K and the pressure of 10 MPa aimed at stabilizing gas hydrates for storage and transportation purposes, sodium dodecyl sulfate (SDS), a kinetic promoter, and hydroxyethyl cellulose (HEC), a stabilizer, were added to the solutions. These additives improved the rate of the formation of gas hydrate and provided stability for storage and transportation at lower pressures.[6] Yevi and Rogers[7] examined the potential of hydrates for storing fuel for natural gas vehicles as an alternative to liquid petroleum-based fuels, driven by environmental considerations. Their findings indicate a storage capacity of 143−159 (v/v) of gas.

The effects of adding surfactants and promoters on hydrate formation, growth rate, and storage capability have been studied widely.[8−10] The incorporation of nanoparticles into hydrate formation experiments has shown promise in amplifying the storage volume of the gas and expediting the hydrate formation kinetics. Owing to the minute size of their particles (<100 nm), nanoparticles possess a substantial surface area per unit mass, leading to a marked enhancement in heat and mass transfer in the liquid, gases, and hydrate phases. This serves to improve the hydrate development by conveying the gas to the hydrate surface simultaneously converting the heat that is produced away from the reaction point. This boosts gas consumption in hydrate formation.[11−14] Pahlavanzadeh et al.[15] used SDS and cetyltrimethylammonium bromide (CTAB) with CuO, SiO_2, and Al_2O_3. The nanoparticles acted as catalysts and promoters in the formation process of CH_4

Received: November 20, 2023
Revised: January 31, 2024
Accepted: January 31, 2024
Published: February 16, 2024

© 2024 The Authors. Published by American Chemical Society

Table 1. Specification and Description of Chemicals Utilized in the Study

chemicals	depiction	CAS number	formula	supplier	purity (vol %)
methane	gas	**74-82-8**	CH_4	Afrox	>99.9
aluminum oxide	<50 nm nanoparticles	1344-28-1	Al_2O_3	Sigma-Aldrich	
copper oxide		1317-38-0	CuO		>90.0
zinc oxide	5 μm powder	1314-13-2	ZnO		
graphene	nanoplatelets	7782-42-5			
sodium dodecyl sulfate	220−350 nm	151-21-3	$CH_3(CH_2)_{11}OSO_3Na$ (SDS)		>99.0
water[a]			H_2O		

[a]Not provided by the supplier.

hydrates at 5.5 MPa and 274.15 K. It was reported that SDS of concentration 500 ppm and CTAB of concentration 700 ppm gave the best results, enhancing the rate constant and the percentage of water converted to gas hydrate. Aliabadi et al.[16] noted that the process of CH_4 hydrate development releases heat, by incorporating CuO nanoparticles into the water. This created an enhanced nanofluid with improved heat transfer capabilities, leading to a more rapid dispersion of heat within the solution. The uniform and swift distribution of heat in the solution facilitated attainment of the optimal temperature needed for enhanced nucleation. Consequently, the presence of nanoparticles can create conditions conducive to promoting nucleation. Moreover, it was observed that a concentration of 0.05 wt % SDS was ideal for stabilizing nanoparticles in solution. Higher concentrations were found to eliminate the influence of nanoparticles, while lower concentrations resulted in precipitation. Therefore, this study used a concentration of 0.05 wt % SDS.[16] Pandey et al.[17] carried out a morphological analysis on the effects of antifoaming agent, silicon which was based on polymeric surfactants to prevent SDS forming in CH_4 gas hydrate dissociation. It was observed that the antifoaming agent had insignificant effects on the CH_4 hydrate formation, since its only purpose was to affect the antifoaming properties of SDS.

Ndlovu et al.[18] observed that graphene nanoplatelets improved CH_4 gas conversion into CH_4 gas hydrate by over 100% when applied in gas hydrate formation. Zhang et al.[19] utilized rhamnolipid, a green surfactant, to promote the formation of CH_4 gas hydrate at varying concentrations, ranging from 0 to 800 ppm. It was noted that the consumption of gas increased as the concentration of rhamnolipid increased, and the interfacial tension was noted to be a significant factor in increasing the rate of hydrate formation. Zhao et al.[20] applied a novel idea of using modified balsa wood as sustainable and environmentally friendly porous media in the formation of CH_4 gas hydrates. This procedure resulted in a reduction by 88%, in the duration required for the initiation of hydrate nucleation. The amount of gas stored increased to 150 (v/v), and it was noted through X-ray microscopy that the flow patterns were improved with the inner channels and linked pores supporting hydrate growth within the inner parts. Inhibitors such as urea, choline chloride, and deep eutectic solvents have been utilized to control the rate of CH_4 hydrate formation. Results obtained showed that the nucleation of CH_4 can be delayed by over 48 h in the presence of choline chloride and urea with reline acting as a thermodynamic and kinetic inhibitor in the presence of deep eutectic solvents.[21] Pandey et al.[22] investigated the formation and dissociation of CH_4/tetrahydrofuran in the presence and absence of 3 wt % NaCl. Morphology changes during hydrate growth, nucleation, and dissociation of the mixed hydrate at different formation pressures of 3 and 5 MPa at 283 K were presented. An upward growth above the gas−liquid interface was observed during the initial stages of hydrate formation. For the nonsaline solution, a downward growth in the liquid−gas interface was observed. Furthermore, dissociation of the saline solution took less time than the nonsaline water with the presence of saline improving heat transfer during dissociation.

Yu et al.[23] investigated the kinetics of CH_4 gas hydrate formation in the presence of cyclopentane (CP). Induction time, gas uptake, and the rate of hydrate formation were reported based on experimental results. It was observed that the CH_4 hydrate was formed in two steps; first, CP hydrate formation followed by CH_4 gas occupying the CP hydrate cavities to form a mixed hydrate of CP and CH_4. Moreover, rapid gas hydrate formation rates were observed with 131.80 mmol/mol H_2O gas uptake in 138 min. The major finding of the study was the high gas uptake at a temperature as high as 298.15 K. Simulations at a molecular level were carried out to investigate the effects of different ratios of water-to-nanoparticle during CH_4 hydrate formation. The study focused on parameters such as gas−water systems, hydrate cage distribution, thermal conductivity, diffusion coefficient, and radial distribution function. It was observed that medium ratios of water/nanoparticles resulted in improved carbon storage and a higher number of cages. Furthermore, the nano-Cu had a high impact on hydrate stability and the thermal conductivity of the gas−water system.[24] Kinetic promoters such as L-tryptophan, L-leucine, L-methionine, and H-SSZ-13 zeolite were utilized in an investigation aimed at improving the gas hydrate formation kinetics in a novel reactor. It was observed that H-SSZ-13 had the lowest rate taking 286 min. It also showed the highest volumetric capacity of 115 v/v at 283 K. The introduction of a fluidized bed reactor (FBR) with metallic filament packing (MFP) light increased the diffusion as well as thermal conductivity leading to 96% and 88% increase in storage capacity of the sII cages at 283 and 293 K, respectively, in the presence of zeolite.[25]

In this study, the effects of CuO and Al_2O_3 nanoparticles, graphene nanoplatelets, and ZnO microparticles on the kinetic formation of CH_4 hydrate were studied experimentally at 4.66 MPa and 275.8 K, for gas storage applications. The pressures selected for the study were lower, and the temperatures were higher than the ones published in the literature. Mohammadi et al.[26] used 7 MPa and 273.65 K, while Ganji et al.[9] utilized 8.23 MPa and 298 K. The pressure of 4.66 MPa was selected since hydrate research seeks to reduce the hydrate formation pressure, hereby reducing costs. Hence, it was deemed appropriate to use the lowest pressure and attempt to improve the kinetic parameters at this point. Furthermore, the study considered the influence of the temperature and pressure on hydrate formation. The induction period, storage volume, rate

https://doi.org/10.1021/acs.energyfuels.3c04584
Energy Fuels 2024, 38, 4480−4491

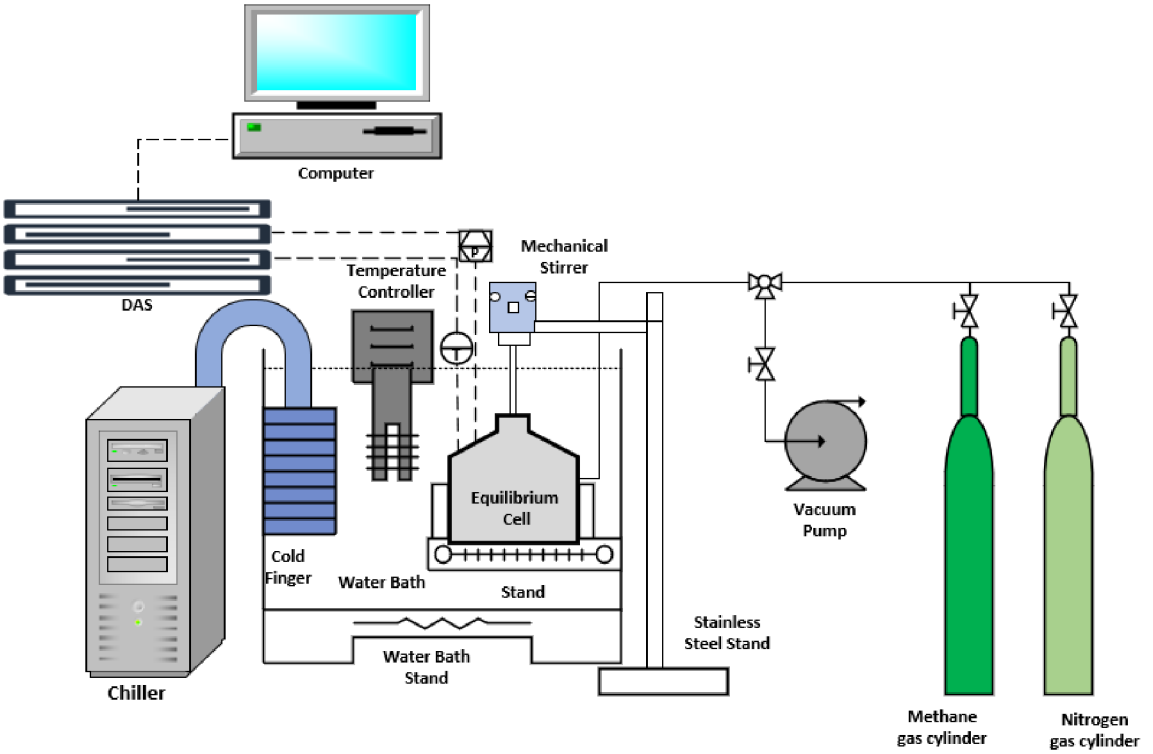

Figure 1. Outlay of the equipment setup utilized in the CH_4 kinetics measurements. (In this diagram, DAS represents Data Acquisition System in a summarized form.)

Chart 1. SmartArt Graphic for the Experimental Technique Utilized

Sample Preparation

- Preparation of 0.05 wt.% SDS solution in a 2000 ml volumetric flask using deionized water. SDS was also used in the preparation of other solutions with different nanofluids for the investigations.
- Weighing of each nanoparticle was performed using an OHAUS PA4202C top pan balance
- Transferring measured nanoparticles to a 50 ml tube containing 20 ml of SDS solution.
- Vigorous blending of the solution for a duration of five minutes using a vortex mixer.[28]

CH_4 hydrate formation

- Opening the cell by removing the top flange and using acetone to clean the cell.
- Addition of 20 cm^3 of the reaction solution to the equilibrium cell and then sealing the reactor.
- Positioning of the cell in a chilled water bath maintained at 275.8 K.
- Evacuating the cell for five minutes to remove any non-condensable gases and air.
- Injection of CH_4 gas into the cell to attain the desired pressure through the use of a back-pressure regulator and a pressure transducer.
- Starting the data logger to monitor the reaction progress, with the stirrer set speed of 220 revolutions per minute. As hydrates began to form within the reactor, the pressure gradually declined until it stabilized at a constant pressure.

of gas consumption, and amount of water incorporated into the hydrate were modeled based on the experimental data measurements at different temperatures and pressure conditions.

2. EXPERIMENTAL SECTION

2.1. Materials. Table 1 provides a record of the substances employed in the study. A precision OHAUS PA4202C top pan balance, accurate to 1.0×10^{-4} g, was utilized for measuring the additives. The deionized water utilized in this research is produced by the Algae portable water filtration system at the University of KwaZulu-Natal laboratories, with a conductivity of 6.4×10^{-1}mS cm^1.

2.2. Apparatus. Figure 1 displays the experimental unit that was used for the study. This equipment has been reported by Ngema et al.[27] in a hydrate study of fluorinated refrigerants. It comprises a 316L stainless steel vessel with an upper pressure limit of 10 MPa, a design size of 52 cm^3, and a usable volume of 36.5 cm^3. The cells' internal stirrer was turned by a motor system that was attached to a shaft with a magnetic tip to accomplish mixing of reactants. The pressure within the equilibrium cell was monitored by a type 1−10 WIKA pressure sensor with a 0−10 MPa rating. An aluminum block that held the pressure sensor was kept at a constant temperature using a TDGC2 variac voltage regulator. Temperature was measured using a class A WIKA thermocouple with a 0.08 K precision. An Agilent 34972A data logging device was utilized to register temperature and pressure every 5 s. The temperature of the bath containing water/ethyl glycol was maintained using a programmable bath controller Polyscience TXF200 model rated over 243.15 to 323.15 K and exterior dimensions of 595 × 460 × 360 mm^3. To immerse the cell in the water bath, a hydraulic jack was employed to raise and lower the water bath. A rotary vane vacuum pump, specifically the RV12 model, was

https://doi.org/10.1021/acs.energyfuels.3c04584
Energy Fuels 2024, 38, 4480−4491

employed to remove air from the equilibrium cell and connecting lines.[28]

2.3. Experimental Technique. The experimental procedure employed in this study is detailed in FlowChart 1, providing a visual representation and step-by-step explanation of the process followed.

2.4. Uncertainty of Measured Variables. The uncertainty in pressure and temperature was determined and reported as a combined expanded uncertainty. The contributing factors considered were instrumental errors, correlation offset, calibration errors, and an offset in repeatability. The expanded uncertainty for pressure was 1×10^{-2} MPa and 1×10^{-1} K for temperature. The uncertainty for time was due to the instrument utilized, a stop watch, which was 0.01s. The expanded mass uncertainty for the solution concentration was 6.0×10^{-2} wt %.

3. KINETIC MODEL

The comprehensive explanation of the model and equations employed in this research to calculate kinetic parameters such as the transformation of water into the hydrate phase, CH_4 gas consumption, hydrate formation speed, and storage capacity (SC) is detailed in Ndlovu,[28] Babaee et al.,[29] Fakir et al.,[30] and Klauda and Sandler.[31] The summary of the expressions used to obtain key parameters is presented below.

The amount of gas consumed during the experiments was calculated using the real gas law in the form of

$$\Delta n_{CO_2} = \frac{P_0 V_0}{Z_0 R T_0} - \frac{P_t V_t}{Z_t R T_t} \quad (1)$$

where P and T represent the pressure and temperature of the vessel, respectively, V is defined as the volume of gas inside the vessel, Z is the compressibility factor calculated from the Valderrama modification of the Patel−Teja equation of state (VPT-EoS),[32] R is the universal gas constant, and subscripts 0 and t indicate conditions of equilibrium cell at time = 0 and time = t, respectively.

Equation 2 expresses the gas usage rate, denoted as $r(t)$, during hydrate formation:

$$r(t) = \frac{n_{CH_4,i-1} - n_{CH_4,i+1}}{(t_{i+1} - t_{i-1}) n_{wo}} \quad (2)$$

where $n_{CH_4,i-1}$ and $n_{CH_4,i+1}$ are the number of moles of methane in the gas phase at t_{i+1} and t_{i-1} which are calculated using the real gas law and n_{wo} is the initial number of moles of water. To estimate the apparent rate constant of the reaction during hydrate formation, the following equation was used:

$$k_{app} = \frac{r(t)}{f^G_{CH_4} - f^G_{equilib}} \quad (3)$$

The storage capacity (SC), defined as the standard volume of gas stored per volume of hydrate, is determined by the equation:

$$SC = \frac{V_{STP}}{V_H} = \frac{n_{CH_4} R T_{STP}/P_{STP}}{V_H} \quad (4)$$

Here, V_H represents the volume of the gas hydrate, and STP refers to standard conditions.

Equation 5 characterizes the water-to-hydrate conversion as the amount of water converted to hydrate per mole of feed

$$\text{Water to hydrate conversion} = \frac{M \times \Delta n_{CH_4}}{n_{w_o}} \quad (5)$$

where M is the hydration number.[29]

4. RESULTS AND DISCUSSIONS

The kinetics of hydrate formation were investigated in this work with uniform conditions in terms of the stirring rate, temperature, and pressure, following the outlined hydrate formation procedure. The results from experimental work were modeled to compute the capacity available for CH_4 storage in the gas hydrate, the rate and amount of gas incorporated into the gas hydrate, and the amount of gas. The effects of pressure were studied in the pressure ranging from 4.66 to 6.16 MPa applied while keeping the temperature constant at 275.8 K. Similarly, the impact of temperature was examined in temperature values between 275.77 and 277.74 K, at a pressure of 4.66 MPa. During these experiments, a steady stirring speed of 220 rpm was kept constant throughout the experiments. This value was selected based on the reactor vessel dimensions to achieve satisfactory mixing.

The discrepancy between the experimental pressure and the pressure on the equilibrium line at the driving force or extent of subcooling is a critical factor. Figure 2 demonstrates that the high pressure of the gas leads to a greater extent of subcooling, ultimately leading to an increased level of hydrate formation.

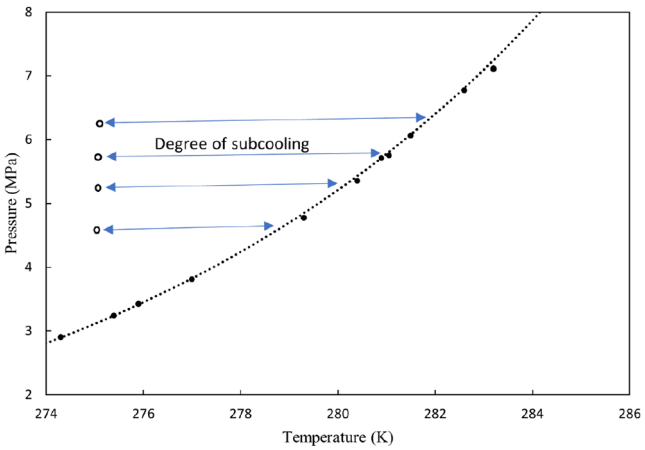

Figure 2. Degree of subcooling between the initial kinetic experimental conditions and CH_4 hydrate equilibrium line.

4.1. Induction Time. The induction period refers to the duration between introducing gas into the cell and emergence of the first hydrate lattice. Figure 3a−d shows the pressure and temperature plotted against time for four systems. The induction time is demarcated by the temperature graph's sharp rise, which coincides with a slight pressure drop as the gas is absorbed into the hydrated matrix.

The induction times for all of the examined systems can be found in Table 2. In general, systems containing nanoparticles exhibited shorter induction times compared to those with ZnO powder. For pure water, the induction time was 18.4 min. The introduction of 0.05 wt % SDS decreased the induction period to 7.9 min. This is caused by the existence of numerous nucleation sites in the solution, which expedited the hydrate formation process.

As depicted in Table 2, the use of nanoparticles resulted in an average induction time of 2 min. Notably, the combination of 0.1 wt % CuO and 0.05 wt % SDS yielded the shortest induction time of 1 min in this investigation. It is worth mentioning that the Al_2O_3 systems exhibited longer induction

https://doi.org/10.1021/acs.energyfuels.3c04584
Energy Fuels 2024, 38, 4480−4491

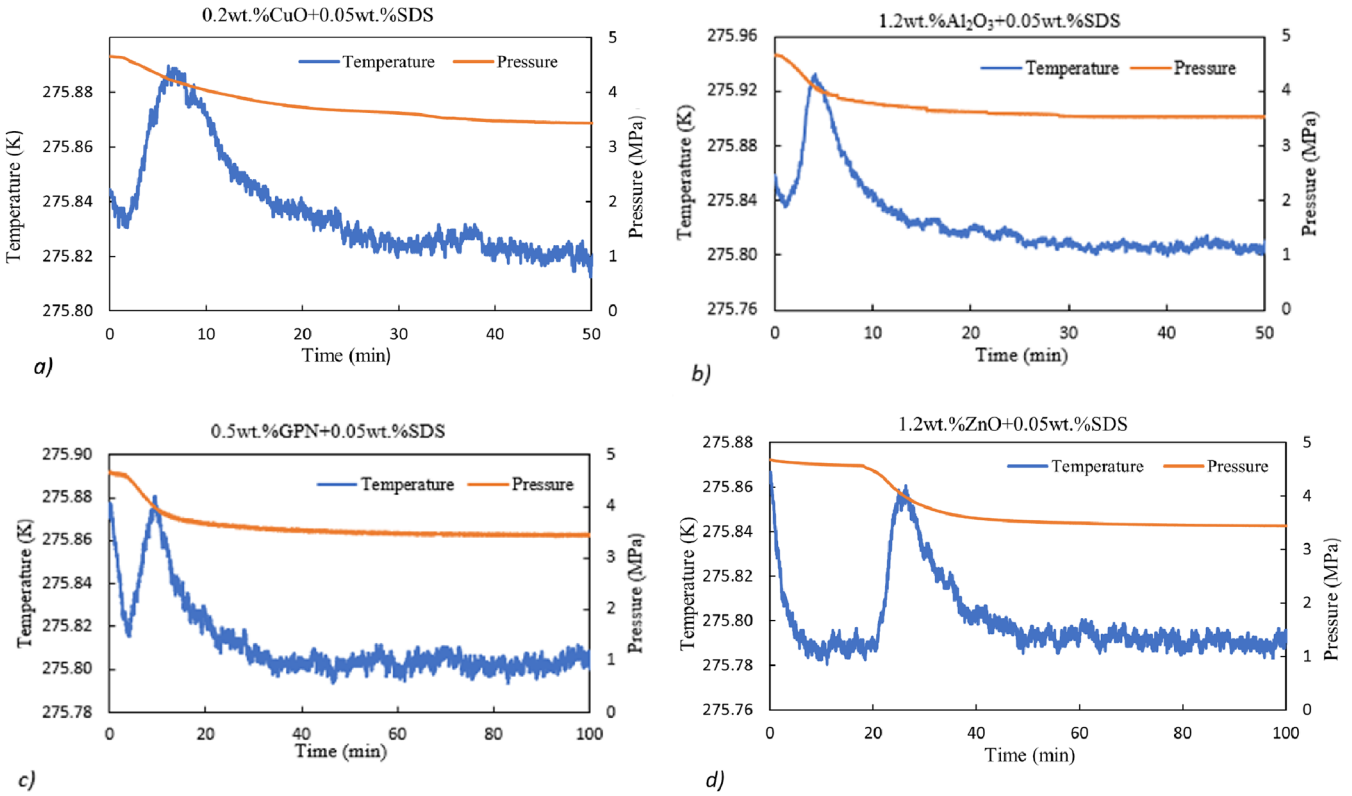

Figure 3. Induction time for CH_4 hydrate in the presence of a) 0.2 wt % CuO + 0.05 wt % SDS, b) 1.2 wt % Al_2O_3 + 0.05 wt % SDS, c) 0.5 wt % GPN + 0.05 wt % SDS, and d) 1.2 wt % ZnO + 0.05 wt % SDS.

Table 2. Time Taken for the Formation of CH_4 Hydrate with the Inclusion of Additives in the Study at Temperature and Pressure Conditions of 275.8 K and 4.66 MPa, respectively[a]

	induction time (min)					
	concentration of additives (wt %)					
reactant	0	0.1	0.2	0.5	1	1.2
deionized water	18.4					
0.05 wt % SDS solution	7.9					
CuO + 0.05 wt % SDS solution		1.0	1.8	3.3	2.3	7.4
Al_2O_3 + 0.05 wt % SDS solution		6.3	10.7	24.7	5.8	1.1
GPN + 0.05 wt % SDS solution		0.9	2.5	4.1	0.1	0.3
ZnO + 0.05 wt % SDS solution		2.9	13.1	5.2	19.1	20.7

[a]Uncertainty $U(P)$ = 0.01 MPa, $U(T)$ = ± 0.1 K, $U(t)$ = 0.01 s, and $U(x)$ = 0.06 wt %.

times compared to other nanofluids. Arjang et al.[12] observed that at a pressure of 5.7 MPa, the induction time of pure water (380.3 min) was reduced to 272.9 min by the addition of trisodium citrate solution and further to 99.2 min with the addition of silver nanoparticles. This is similar to the findings in this work as nanoparticles had the lowest induction time of 1.0 s, followed by 0.05 wt % SDS solution with an induction time of 7.9 min then distilled water with the longest induction time of 18.4 min. The mixture of nanoparticles and SDS resulted in the shortest induction time as the surface tension of water had been reduced by SDS making it easy for nanoparticles to enhance hydrate formation.

4.2. Gas Consumption. Gas consumption calculations were used to ascertain the quantity of gas used during the hydrate formation phase. The determination of this parameter was facilitated using eq 1, as outlined in the kinetic model discussed in Section 3. Within this model, the calculation of gas consumption involved noting the number of moles in the equilibrium cell at a certain time period and taking a difference from the initial number of moles of the gas. Consequently, the total gas consumed was derived by subtracting the initial quantity of moles in the gas phase from the remaining moles at a specific time in the gas phase. This difference is the number of moles consumed in gas hydrate formation. Referring to Figure 4a, the number of CH_4 moles utilized in the hydrate formation process rises as the temperature decreases. The lowest consumption was noted at an apex temperature of 277.74 K, whereas the highest consumption occurred at a temperature of 275.77 K. Figure 4b illustrates that gas consumption peaked at a pressure of 6.16 MPa and reached its lowest pressure of 4.66 MPa.

Figure 5a–d shows the gas consumption during the formation of CH_4 hydrate obtained using the chemical additives employed in this investigation. Figure 5a–c shows the effects of nanoparticles, while Figure 5d shows the influence of ZnO microparticles on CH_4 hydrate formation. The behavior of the systems with different nanoparticles at the same concentration is shown to be different in Figure 5a,b. The highest gas consumption was obtained with CuO in Figure 5a with 0.1 wt %, while the lowest was obtained with pure water and 0.05 wt % SDS solution. In all systems utilizing nanoparticles, the amount of CH_4 consumed during hydrate formation surpassed that of deionized water and solution 0.05 wt % SDS. As shown in Figure 5b, the system with 1.2 wt %

https://doi.org/10.1021/acs.energyfuels.3c04584
Energy Fuels 2024, 38, 4480–4491

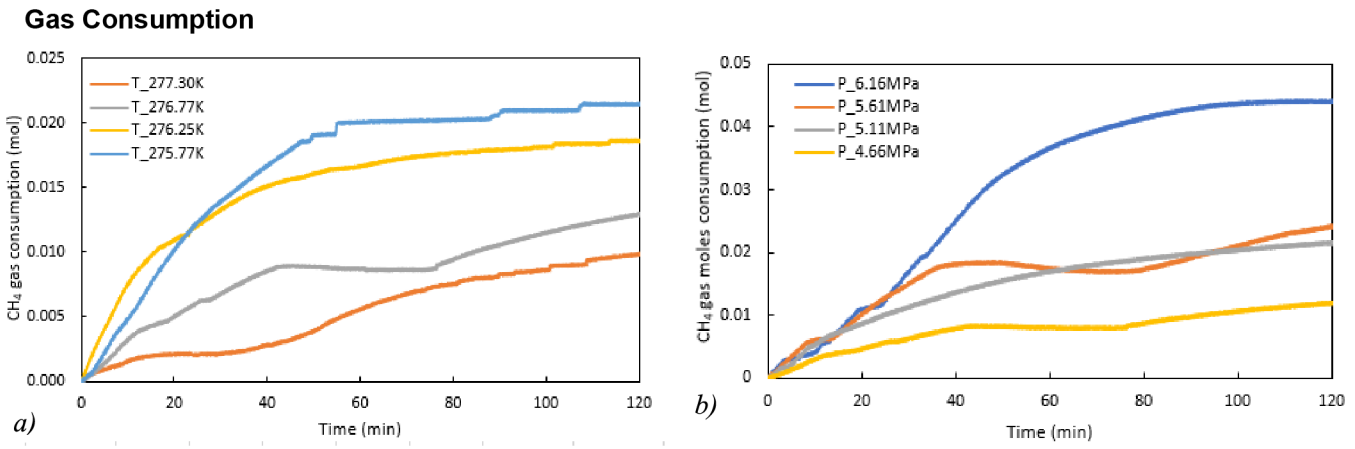

Figure 4. Amount of CH_4 moles consumed during hydrate formation at different initial temperatures and pressure conditions. a) Temperature variation at a constant pressure of 4.66 MPa. b) Pressure variation at a constant temperature of 275.8 K.

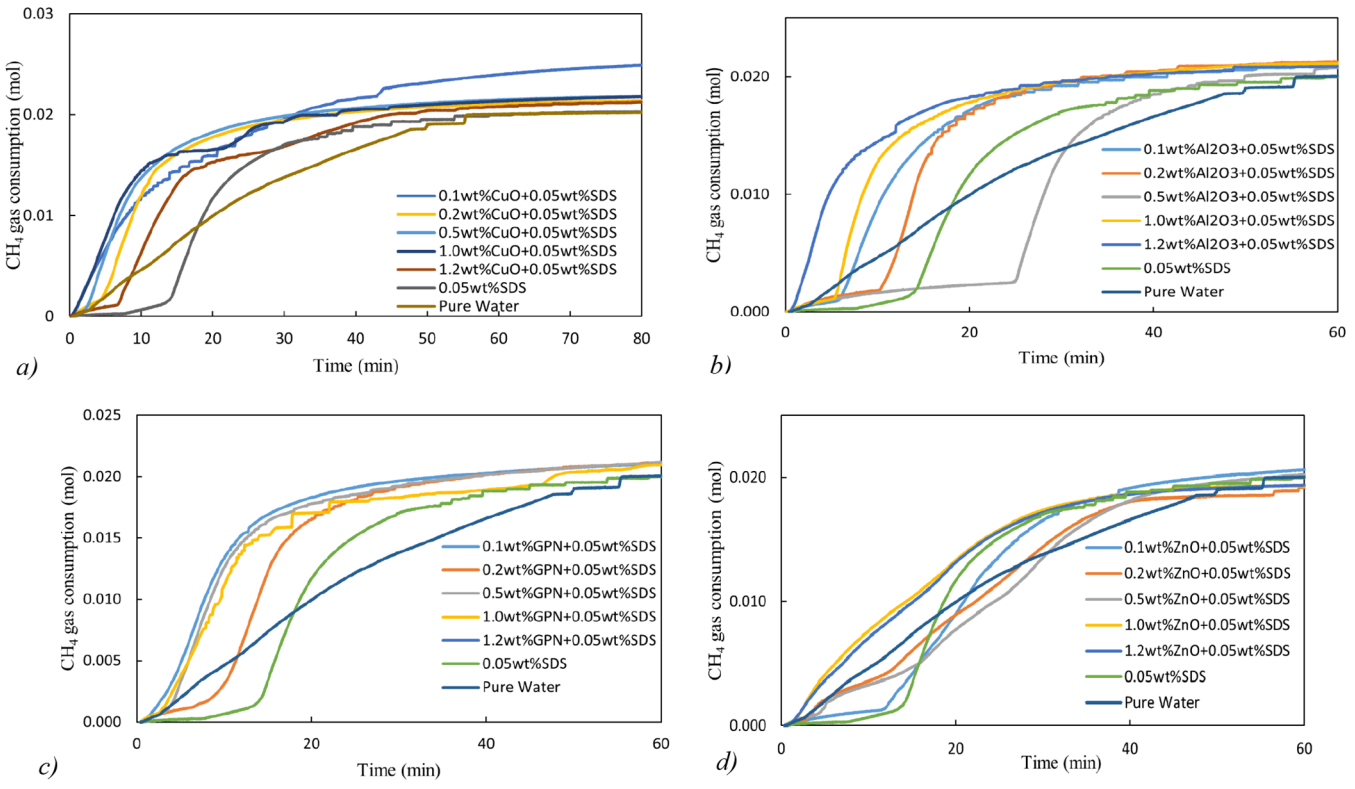

Figure 5. Quantity of CH_4 moles consumed during hydrate formation in the presence of different additives. a) Copper oxide (CuO) nanoparticles, b) aluminum oxide (Al_2O_3) nanoparticles, c) graphene nanoplatelets, and d) zinc oxide (ZnO) powder at 275.8 K and 4.66 MPa in concentrations specified in the graphs.

Al_2O_3 nanoparticle solution was the only system that exhibited a higher gas consumption rate than the pure water solution, while the remaining systems studied exhibited a lower gas consumption rate.

Figure 5c shows the gas consumption obtained with the graphene nanoplatelets. The total gas consumption was relatively similar for all graphene nanoplatelet concentrations measured in the study. However, the gas consumption rate was faster than pure water and 0.05 wt % SDS. Figure 5d shows the gas consumption in the system containing ZnO crystals. The trends indicate extended induction times, and the pace of formation of hydrates was noted to be less rapid compared to deionized water in all instances, except for the system containing 0.1 wt % ZnO. The gas consumption rate with ZnO systems was found to be lower when compared to nanofluids. This can be attributed to the relatively larger ZnO particle sizes, which clogs the pathways in hydrate cages, preventing continuous hydrate growth. In a similar investigation, Ganji et al.[9] performed experiments at 8.3 MPa and 268.2 K, reporting that the moles of CH_4 consumed with 500 ppm of SDS + 300 ppm Xanthan solution were 0.5 mol in a period of 8 h while Arjang et al.[12] reported that 0.019 mol of CH_4 gas were consumed after 15 h. In this study, a solution of 0.1 wt % CuO + 0.05 wt % SDS resulted in CH_4 gas consumption of 0.0238 mol in 1 h. Hence, in this comparison

https://doi.org/10.1021/acs.energyfuels.3c04584
Energy Fuels 2024, 38, 4480−4491

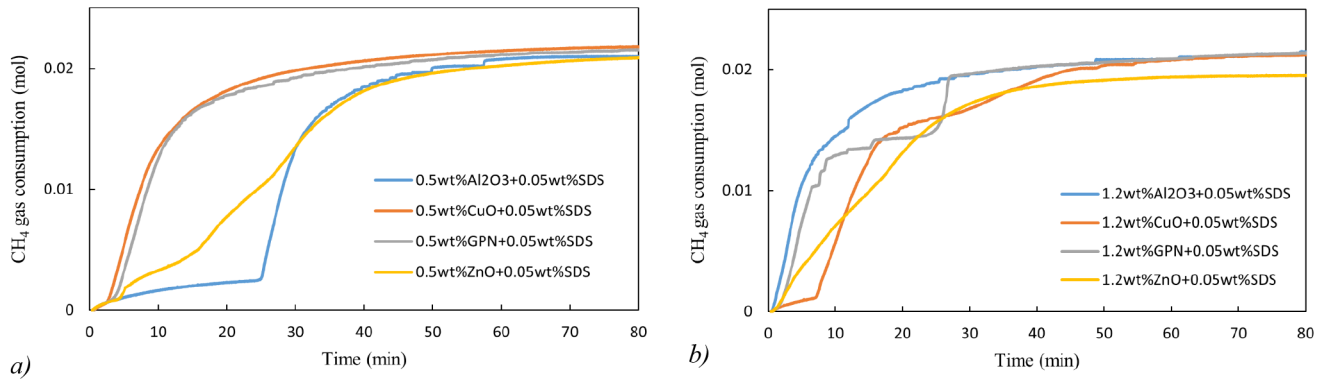

Figure 6. Comparison of amount of gas consumed for Al_2O_3 and CuO nanoparticles, ZnO powder and Graphene nanoplatelets at additives with 0.05 wt % SDS at concentrations of a) 0.5 wt % and b) 1.2 wt % at 275.8 K and 4.66 MPa.

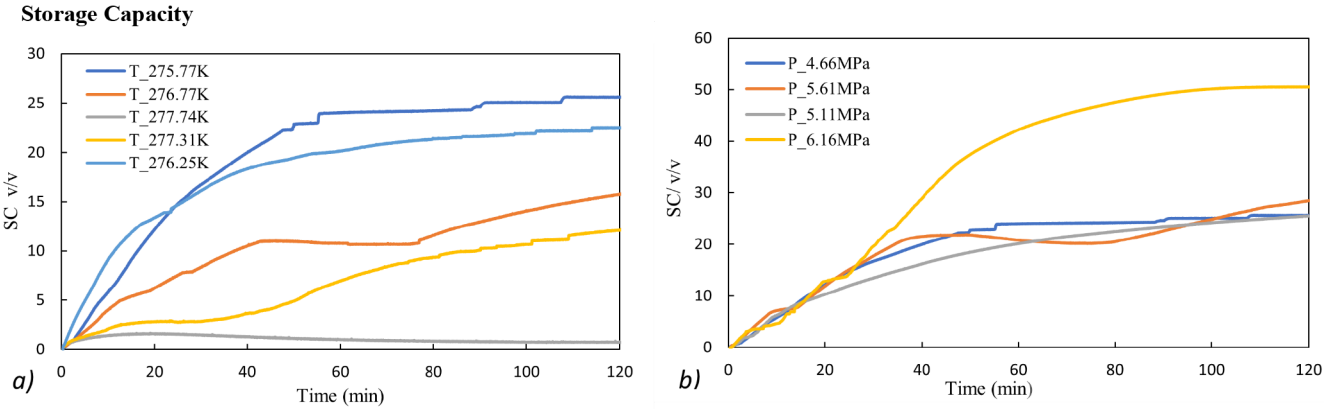

Figure 7. Storage capacity for CH_4 hydrate formation at different initial temperatures and pressure conditions. a) temperature variation at a constant pressure of 4.66 MPa and b) pressure variation at a constant temperature of 275.8 K.

regardless of the difference in pressures, nanoparticles improved the efficiency of the hydrate formation process.

In Figure 6, a comparison of the gas consumption for different systems is shown. For this comparison, 0.5 and 1.2 wt % of nanoparticles were selected. It is demonstrated that the utilization of nanoparticles led to heightened gas consumption in comparison to the use of ZnO microparticles across varying concentrations of 0.5 and 1.2 wt %. This outcome aligns with the anticipated behavior, given that nanoparticles have demonstrated a capacity to enhance both hydrate formation rates and gas consumption. The Supporting Information includes an evaluation of repeatability in gas consumption.

4.3. Storage Capacity. The storage capacity is defined as the standard volume of gas stored per hydrate volume. The impact of temperature on the storage capability was determined for the condition of the pressure that exhibited the lowest gas consumption (4.66 MPa). The temperature was varied five times from 275.77 to 277.30 K, as shown in Figure 7a, at a constant pressure of 4.66 MPa. At the lowest temperature of 275.77 K, the system achieved a maximum storage volume of 25.61 v/v, whereas at the peak temperature of 277.74 K, the capacity dropped to a minimum of 0.75 (v/v). This demonstrates a noticeable reduction in the volume available for gas storage as the temperature increases, resulting from the temperature entering the stable hydrate region.

Figure 7b shows the effects of pressure variation on storage capacity with the pressure varied from 4.66 to 6.16 MPa. The maximum storage was obtained at 6.16 MPa with a value of 50.52 (v/v). The storage capacity observed within the pressure range of 4.66 to 5.61 MPa was consistently similar across all the pressure conditions studied, averaging at approximately 26.5 (v/v) for every system. The general trend was an increase in storage capacity as the pressure increases. The impact of additives on the storage capacity is demonstrated in Figure 8a–d at a pressure of 4.66 MPa. Figure 8a displays the outcomes of the storage capacity for the CuO + SDS system at various concentrations. The peak storage capacity achieved was 28.5 (v/v) with the lowest concentration used, which is 0.1 wt % CuO + 0.05 wt % SDS. As the concentration of nanoparticles increased, the storage capacity was noted to decrease. The system comprising pure water and 0.05 wt % SDS exhibited the lowest storage capacity. In Figure 8b, where Al_2O_3 was utilized, there is no observable trend though nanoparticles behaved better than pure water and 0.05 wt % SDS solution. Graphene nanoplatelets exhibited a comparable pattern, as depicted in Figure 8c. In Figure 8d, the zinc oxide system displayed a behavior akin to systems with nanoparticles, maintaining an average storage capacity of 25 (v/v). With zinc oxide microparticles, there is a clear trend in the graphs, with 0.1 wt % ZnO having the maximum storage volume of 25.86 (v/v). As can be seen in Figure 8a, the 0.5 wt % CuO + 0.05 wt % SDS was repeated twice, and the resulting plots were similar and within the experimental error.

4.4. Water to Hydrate Convention. The conversion of water to hydrate represents the proportion of water moles transformed into hydrate per mole of feed. Analyzing Figures 9a,b and 10a–d, it is evident that the patterns observed for water-to-hydrate conversion closely mirror those seen in

https://doi.org/10.1021/acs.energyfuels.3c04584
Energy Fuels 2024, 38, 4480–4491

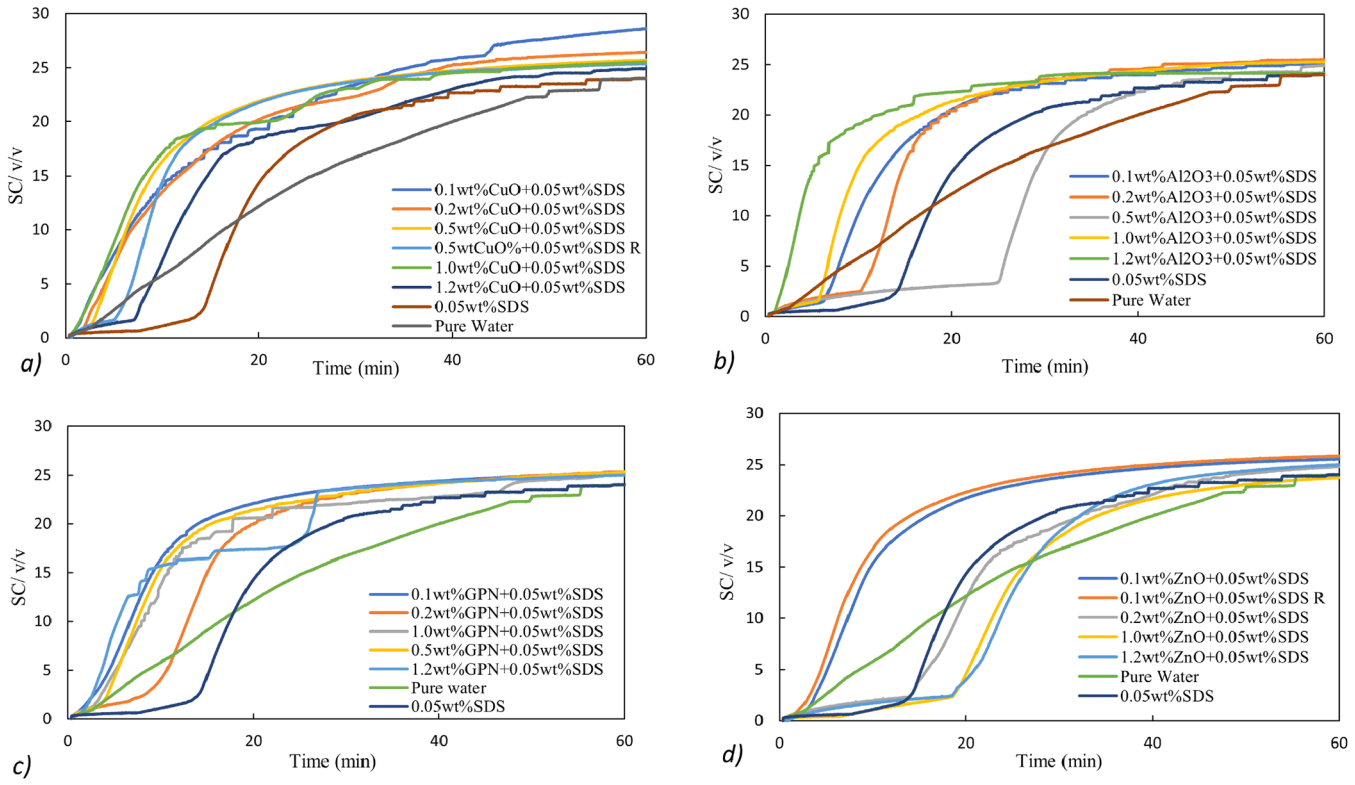

Figure 8. Amount of CH_4 gas stored in hydrate formation in the presence of a) copper oxide (CuO) nanoparticles, b) aluminum oxide (Al_2O_3) nanoparticles, c) graphene nanoplatelets, and d) zinc oxide (ZnO) powder, at 275.8K and 4.66 MPa in concentrations specified in the graphs; SDS R = repeat.

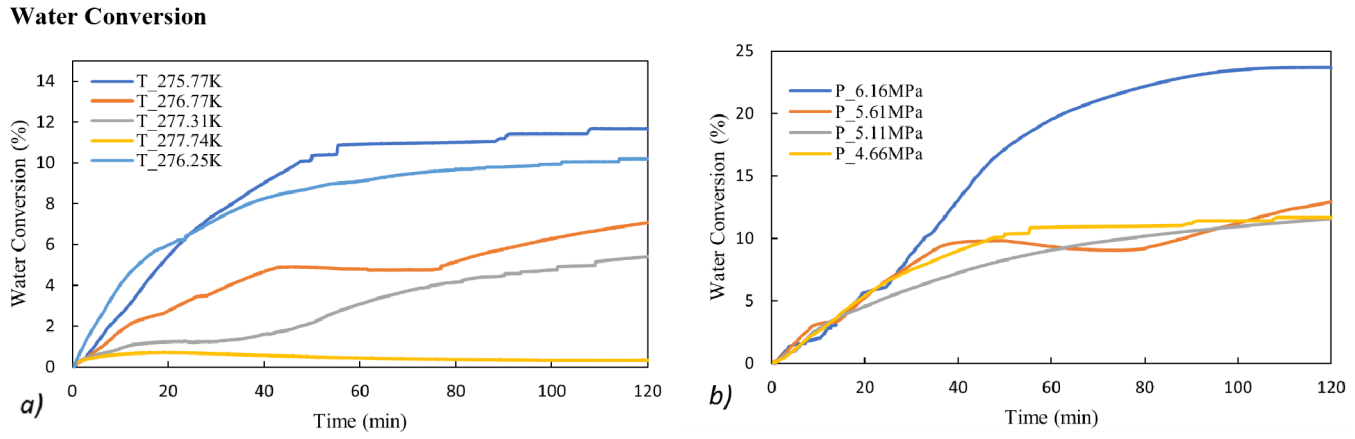

Figure 9. Water-to-hydrate conversion during CH_4 hydrate formation: a) temperature variation at a constant pressure of 4.66 MPa and b) pressure variation at a constant temperature of 275.8 K.

storage capacity. This similarity arises from the fact that a specific quantity of water is necessary during the incorporation of gas during the formation of the hydrate structure.

For hydrate application in gas storage, it is preferable to utilize minimal water to improve or increase the capacity for gas encapsulation. However, gas molecules are stored in a water lattice. For the combustion application of CH_4 gas, it is preferential to have little water and maximum CH_4 gas to increase the hydrate's heating value or energy value.

4.5. Rate of Gas Uptake. The gas uptake rate pertains to the proportion of gas consumed in relation to the moles of water. When examining Figure 11a,b, as well as 12a–d, it becomes clear that the introduction of nanoparticles leads to an acceleration in the reaction rate.

The gas absorption rate decreases as the temperature rises, as demonstrated in Figure 11a. At a temperature of 276.25 K, the highest gas absorption rate reached 2.7×10^{-4} mol G mol $W^{1-}min^{-1}$. The lowest recorded values were at 5.0×10^{-4} mol G mol $W^{1-}min^{-1}$. This aligns with the information presented in Figure 2, where the impetus for hydrate formation diminishes with an increasing temperature. Similarly, Figure 11b illustrates that the rate of gas absorption decreases with declining pressure. The highest gas uptake rate, at 3.17×10^{-4} mol G mol $W^{1-}min^{-1}$, was achieved at 6.16 MPa, while the lowest rate, 1.0×10^{-4} mol G mol $W^{1-}min^{-1}$, was observed at 4.66 MPa.

Figure 12a shows trends obtained in the system containing CuO nanoparticles. The highest gas uptake rate of 8.9×10^{-4}

https://doi.org/10.1021/acs.energyfuels.3c04584
Energy Fuels 2024, 38, 4480–4491

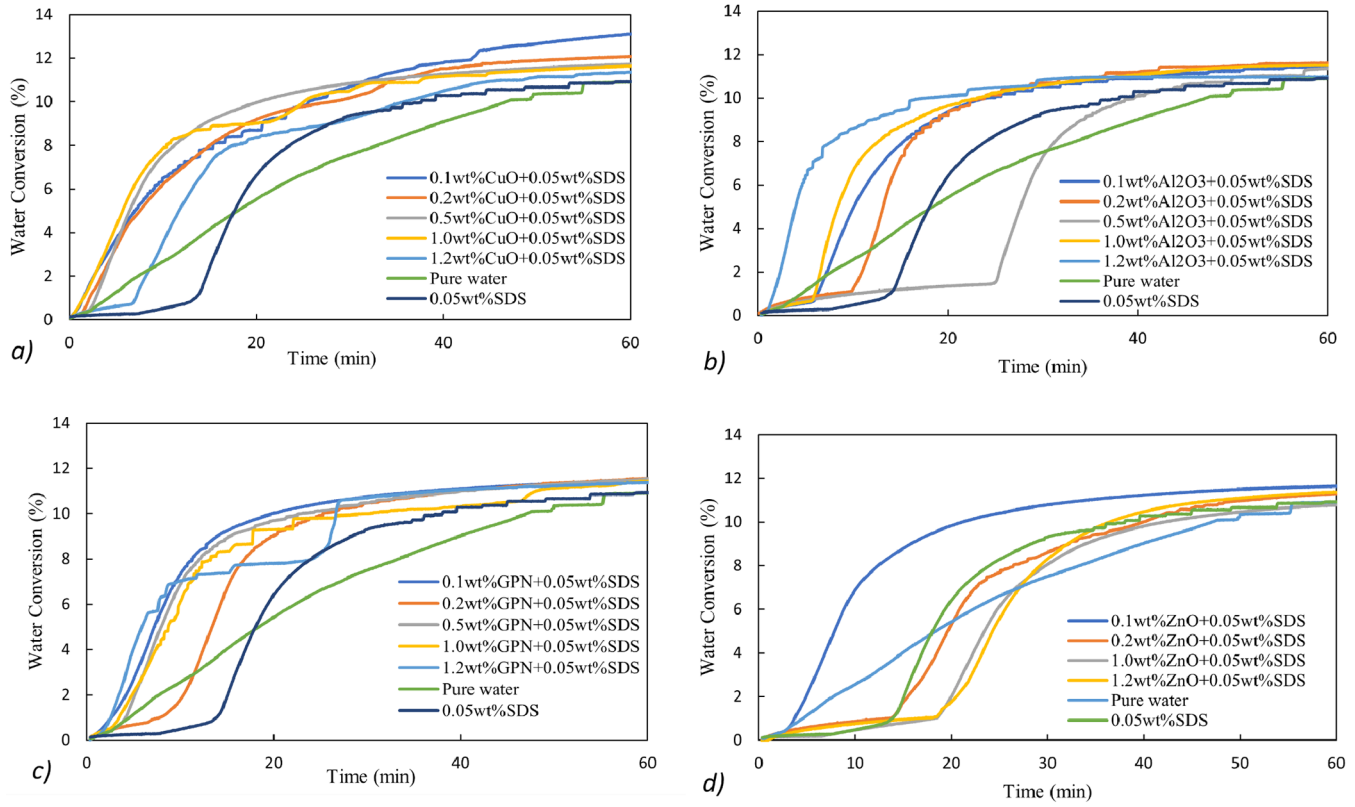

Figure 10. Percentage of water to CH_4 hydrate conversion in the presence of a) copper oxide (CuO) nanoparticles, b) aluminum oxide (Al_2O_3) nanoparticles, c) graphene nanoplatelets, and d) zinc oxide (ZnO) powder, at the temperature of 275.8 K and pressure of 4.66 MPa in concentrations specified in the graphs.

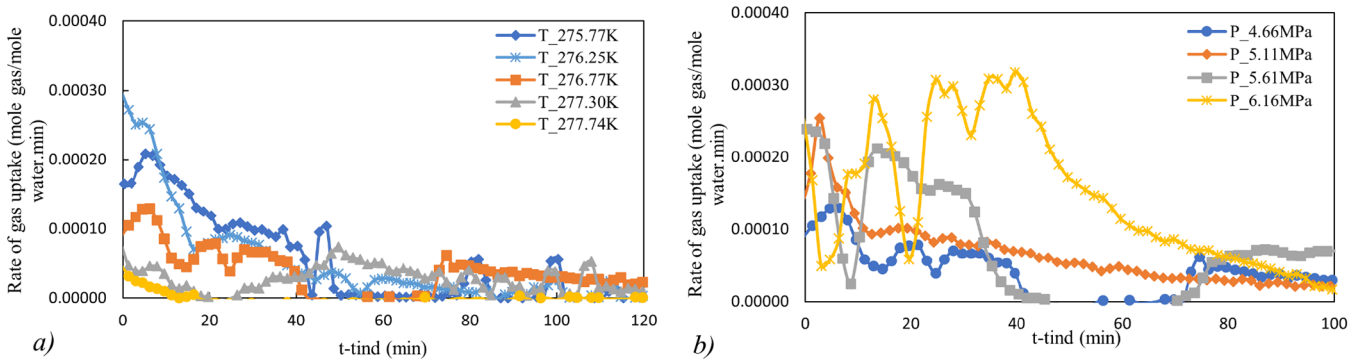

Figure 11. Rate of CH_4 consumption over a given induction time (t-tind) during hydrate formation at different initial temperatures and pressure conditions: a) temperature variation at a constant pressure of 4.66 MPa and b) pressure variation at a constant temperature of 275.8 K. "t-tind" denotes the time of the reaction following the induction period.

mol G mol $W^{1-}min^{-1}$ was achieved with the combination of 0.5 wt % CuO + 0.05 wt % SDS. Meanwhile, both systems with 0.05 wt % SDS and 1.0 wt % CuO + 0.05 wt % SDS exhibited a gas uptake rate of 6.5 × 10^{-4} mol G mol $W^{1-}min^{-1}$. On the contrary, pure water exhibited the lowest gas uptake rate at 2.0 × 10^{-4} mol G mol $W^{1-}min^{-1}$. Thus, the inclusion of SDS and CuO substantially enhanced the gas uptake rate. In Figure 12b, the variation of gas uptake in the system containing Al_2O_3 nanoparticles is presented. This system exhibited the highest gas uptake rates. The highest rate achieved was 1.0 × 10^{-3} mol G mol $W^{1-}min^{-1}$ with 1.2 wt % Al_2O_3 + 0.05 wt % SDS. Following closely, the next highest gas uptake rate was 9.3 × 10^{-4} mol G mol W^{1-} min^{-1} with 1.0 wt % Al_2O_3 + 0.05 wt % SDS, while the rates of consumption for the 0.5 wt % Al_2O_3 + 0.05 wt % SDS and 0.2 wt % + 0.05 wt % SDS systems were relatively higher than the other particulate systems studied at similar compositions. In Figure 12c, graphene nanoparticles show a similar rate of gas uptake for all of the concentrations studied. The rate of gas uptake was between 6.0 × 10^{-4} and 8.0 × 10^{-4} mol G mol $W^{1-}min^{-1}$. In Figure 12d, ZnO microparticles had the highest value of 6.3 × 10^{-3} mol G mol $W^{1-}min^{-1}$ obtained with 0.1 wt % ZnO + 0.05 wt % SDS. The remaining concentration, along with 0.05 wt % SDS, showed similar rates of gas uptake, approximately 6.0 × 10^{-3} mol G mol $W^{1-}min^{-1}$. Mohammadi et al.[26] obtained a gas uptake of 0.1476 (mol/mol) with SDS (500 ppm) at 7 MPa and 273.65 k which was higher than the values of 6 × 10^{-5} mol G mol $W^{1-}min^{-1}$ obtained with 0.05 wt % SDS in this study.

https://doi.org/10.1021/acs.energyfuels.3c04584
Energy Fuels 2024, 38, 4480−4491

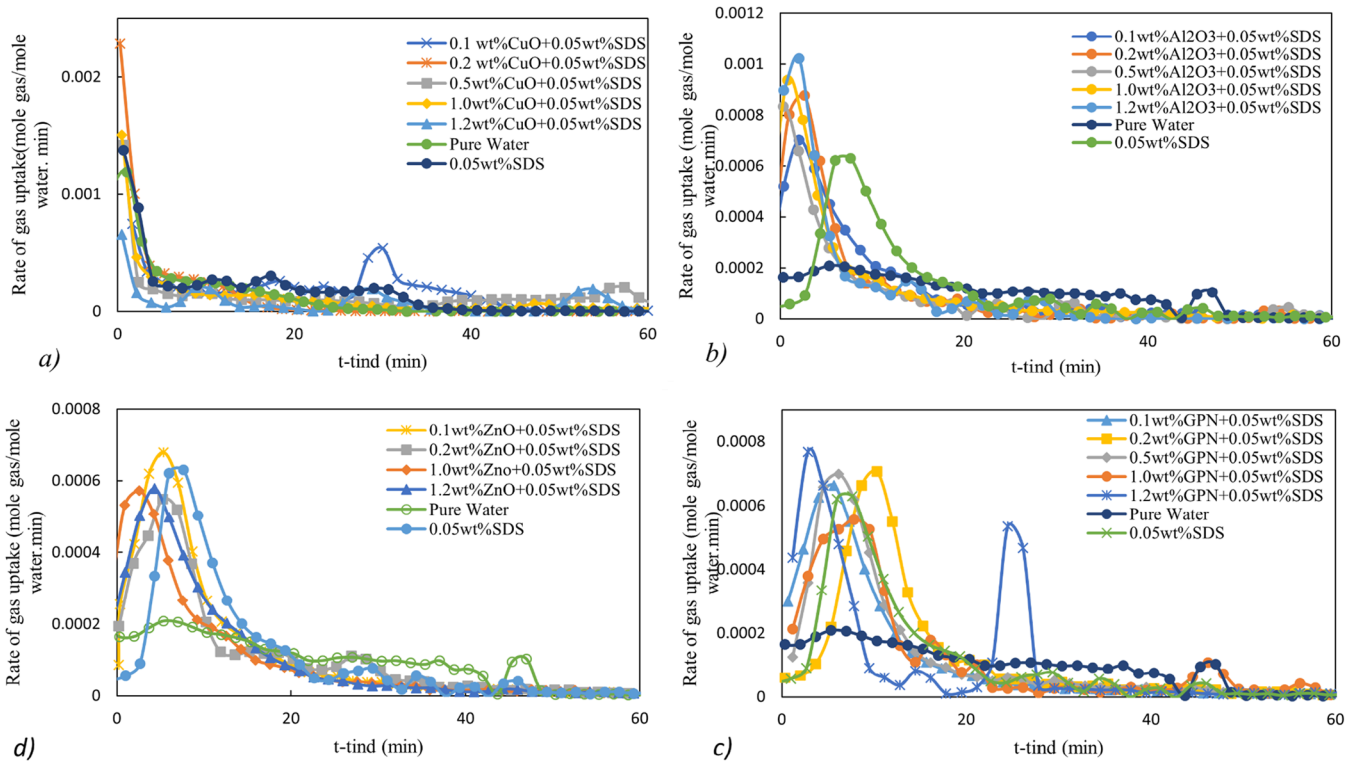

Figure 12. Rate of CH_4 gas consumption over a given induction time (t-tind) during the CH_4 hydrate formation for a) copper oxide (CuO) nanoparticles, b) aluminum oxide (Al_2O_3) nanoparticles, c) graphene nanoplatelets, and d) zinc oxide (ZnO) powder at an initial temperature of 275.8 K and a pressure of 4.66 MPa. "t-tind" denotes the time of the reaction following the induction period.

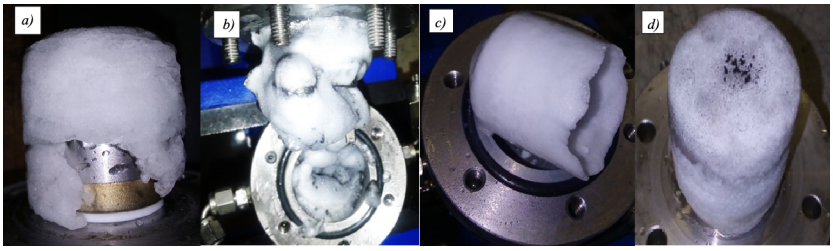

Figure 13. Pictorial view of gas hydrates formed with CH_4 and a) pure water, b) 0.1 wt %ZnO + 0.05 wt %SDS, c) 1.2 wt %Al_2O_3 + 0.05 wt %SDS, and d) 0.5 wt % CuO + 0.05 wt %SDS.

Also, Ag (0.000045 M + SDS (500 ppm) had a gas uptake of 0.133 (mol/mol) while in this study the best system reported was 1.0×10^{-3} mol G mol $W^{1-}min^{-1}$ with 1.2 wt % Al_2O_3 + 0.05 wt % SDS. The high value reported in the literature might be due to higher pressure and low temperature set points used which favor natural gas occurrence leading to a high rate of gas uptake. Overall, a trend similar to that in these two studies was that the rate of gas uptake increased with the addition of SDS and nanoparticles.

5. APPLICATION OF CH_4 HYDRATES

This study exhibits that with the use of chemical additives and nanoparticles, the hydrate storage capacity can be increased. Figure 13a is a pictorial representation of the hydrates from Figure 13a deionized water, Figure 13b, 0.1 wt % ZnO + 0.05 wt % SDS, Figure 1c, 1.2 wt % Al_2O_3 + 0.05 wt % SDS, and Figure 13d, 0.5 wt % CuO + 0.05 wt % SDS.

Improvement in the hydrate formed is shown in Figure 8a–d on storage capacity. Due to their energy values, methane gas hydrates can potentially be utilized for domestic purposes such as lighting and heating. A crucial step is to investigate and come up with means of controlling hydrate decomposition and, hence, the rate of gas release from the hydrate structure. Additives such as methanol act as chemical inhibitors, reducing the rate of CH_4 hydrate dissociation and controlling its decomposition rate.[33] The energy released from the disintegration of the clathrate structure of the hydrate can be employed in the refrigeration process and for coldstorage.[34]

6. CONCLUSIONS

The kinetic and catalytic effects of nanoparticles and chemical additives on the formation of CH_4 hydrate were investigated in this work. The main focus was on the induction period, storage volume, rate of gas absorption, amount of water converted to the hydrate, and gas consumption. Overall, the solution containing nanoparticles demonstrated enhanced thermal properties, shorter induction times, and improved hydrate formation. Of particular importance was the assessment of storage capacity, as it provides an energy store for hydrate utilization for various domestic purposes. The 0.1 wt % CuO +

https://doi.org/10.1021/acs.energyfuels.3c04584
Energy Fuels 2024, 38, 4480−4491

0.05 wt % SDS had the highest storage capacity from all the additive-containing systems studied. The systems of graphene nanoplatelets had, on average, the lowest induction time for all the systems utilized. The system containing Al_2O_3 nanoparticles had a longer induction time compared to other nanoparticles, but the gas uptake rates were the highest of all the systems investigated. The use of ZnO microparticles do not show considerable improvement in the analysis, which further proves that nanoparticles improve hydrate formation. However, ZnO in low concentration had favorable effects on the investigated kinetic parameters. High-pressure conditions were favorable for the parameters studied, but it is uneconomical. The application of hydrates for domestic heating and lighting is a near possibility. An essential aspect of utilizing hydrates is effectively regulating the rate at which hydrate dissociation occurs in order to deliver energy at a desirable rate.

■ ASSOCIATED CONTENT

Supporting Information

The Supporting Information is available free of charge at https://pubs.acs.org/doi/10.1021/acs.energyfuels.3c04584.

To assess the repeatability of experimental measurements, induction times were measured for four selected systems, with each experiment repeated twice for enhanced reliability. The obtained results are meticulously detailed in Table S.1 and visually represented in Figures S.1 to S.4. This systematic approach to repeated measurements not only validates the consistency of the experimental data but also provides a comprehensive overview of the repeatability across the selected systems, contributing to the robustness and reliability of the study (PDF)

■ AUTHOR INFORMATION

Corresponding Author

Saeideh Babaee − *Department of Chemical and Metallurgical Engineering, University of the Witwatersrand, Johannesburg 2000, South Africa;* orcid.org/0000-0003-2412-8618; Email: saeideh.babaee@witz.ac.za

Authors

Phakamile Ndlovu − *Thermodynamics Research Unit, School of Engineering, University of KwaZulu-Natal, Durban 4041, South Africa; Minerals Processing Division, Mintek, Randburg 2125, South Africa*

Paramespri Naidoo − *Thermodynamics Research Unit, School of Engineering, University of KwaZulu-Natal, Durban 4041, South Africa; Department of Chemical Engineering, Banhoekweg,, Stellenbosch University, Western Cape 7600, South Africa;* orcid.org/0000-0002-2724-7308

Kuveneshan Moodley − *Thermodynamics Research Unit, School of Engineering, University of KwaZulu-Natal, Durban 4041, South Africa;* orcid.org/0000-0003-1544-3624

Complete contact information is available at: https://pubs.acs.org/10.1021/acs.energyfuels.3c04584

Notes

The authors declare no competing financial interest.

■ ACKNOWLEDGMENTS

This study was funded by South Africa National Research Fund Grant UID 118606 and the Thermodynamics Research Unit in the School of Engineering at the University of KwaZulu Natal.

■ REFERENCES

(1) Zheng, J.; Chong, Z. R.; Qureshi, M. F.; Linga, P. Carbon dioxide sequestration via Gas hydrates: A potential pathway toward decarbonization. *Energy Fuels* **2020**, *34*, 10529−10546.

(2) Ruffine, L. E. Exploring methane-hydrate formation and dissociation in geologic materials through laboratory experiments: Kinetic behaviour and morphology. *Fuels* **2015**, *141*, 173−184.

(3) Lovedy, J. S.; Nelmes, R. J. High-pressure gas hydrates. *Phys. Chem. Chem. Phys.* **2008**, *10*, 937−950.

(4) Matizakurima, F.; Babaee, S.; Hashemi, H.; Naidoo, P. Separation of Xenon from Noble gas mixtures of Argon, Krypton, and Xenon using gas hydrate technology. *Ind. Eng. Chem. Res.* **2023**, *62* (36), 14484−14496.

(5) Ruppel, C. Methane hydrates and the future of natural gas; MITEI natural gas Report, supplementary paper on Methane Hydrates, 2011; 25

(6) Nazari, K.; Taheri, Z.; Mehrabi, M.; Khodafarin, R. Natural Gas Hydrate Production and Transportation. In *Proceedings of the 7th International Conference on Gas Hydrates (ICGH 2011)*; Hydrafact Ltd: Edinburgh, Scotland, United Kingdom, 2011.

(7) Yevi, G. Y.; Rogers, R. E. Storage of fuels in hydrates for Natural Gas Vehicles (NGVs). *J. Energy Resour. Technol.* **1996**, *118*, 209−213.

(8) Babaee, S.; Hashemi, H.; Mohammadi, A. H.; Naidoo, P.; Ramjugernath, D. Kinetic and thermodynamic behavior of CF_4 clathrate hydrates. *J. Chem. Thermodyn.* **2015**, *81*, 52−59.

(9) Ganji, H.; Manteghian, M.; Sadaghiani zadeh, K.; Omidkhah, M. R.; Mofrad, H. R. Effect of different surfactants on methane hydrates formation rate, stability and storage capacity. *Fuel* **2007**, *86*, 434−441.

(10) Karimi, R.; Varaminian, F.; Izadpanah, A. A.; Mohammadi, A. H. Effects of different surfactants on the kinetics of ethane-hydrate formation: experimental and modeling studies. *Energy Technol.* **2013**, *1*, 530−536.

(11) Park, S.-S.; An, E.-J.; Lee, S.-B.; Chun, W.-G.; Kim, N.-J. Characteristics of methane hydrate formation in carbon nanofluids. *J. Ind. Eng. Chem.* **2012**, *18*, 443−448.

(12) Arjang, S.; Manteghian, M.; Mohamma, A. Effects of synthesized silver nanoparticles in promoting methane hydrate formation at 4.7 and 5.7 MPa. *Chem. Eng. Res. Des.* **2013**, *91*, 1050−1054.

(13) Ndlovu, P.; Babaee, S.; Naidoo, P. Review on CH_4-CO_2 replacement for CO_2 sequestration and CH_4/CO_2 hydrate formation in porous media. *Fuel* **2022**, *320*, 123795.

(14) Najibi, H.; Shayegan, M. M.; Heidary, H. Experimental investigation of methane hydrate formation in the presence of copper oxide nanoparticles and SDS. *J. Nat. Gas Sci. Eng.* **2015**, *23*, 315−325.

(15) Pahlavanzadeh, H.; Khanlarkhani, M.; Rezaei, S.; Mohammadi, A. Experimental and modelling studies on the effects of nanofluids (SiO_2, Al_2O_3, and CuO) and surfactants (SDS and CTAB) on CH_4 and CO_2 clathrate hydrates formation. *Fuel* **2019**, *253*, 1392−1405.

(16) Aliabadi, M.; Rasoolzadeh, A.; Esmaeilzadeh, F.; Alamdari, A. Experimental Study of Using CuO Nanoparticles as a Methane Hydrate Promoter. *J. Nat. Gas Sci. Eng.* **2015**, *27*, 1518−1522.

(17) Pandey, G.; Bhattacharjee, G.; Veluswamy, H. P.; Kumar, R.; Sangwai, J. S.; Linga, P. Alleviation of foam formation in a surfactant driven gas hydrate system: Insights via a detailed morphological study. *ACS Appl. Energy Mater.* **2018**, *1* (12), 6899−6911.

(18) Ndlovu, P.; Babaee, S.; Naidoo, P. Experimental study of CH_4-CO_2 replacement in gas hydrates in the presence of nitrogen and graphene nanoplatelets. *J. Mol. Liq.* **2023**, *371*, 121109.

(19) Zhang, Y.; Zhang, J.; Xu, X.; Liu, W.; Xu, Y.; Yang, M.; Song, Y. The effects of rhamnolipid on the formation of CH4 hydrate and separation of CH_4/N_2 via hydrate formation. *Fuel* **2024**, *357*, 129873.

(20) Zhao, Y.; Qu, A.; Yang, M.; Dong, H.; Ge, Y.; Li, Q.; Liu, Y.; Zhang, L.; Liu, Y.; Song, Y.; Zhao, J. Modified balsa wood with natural, flexible porous structure for gas storage. *Appl. Energy* **2024**, *353*, 122026.

(21) Khoo, Y. Z.; Ho, Y. H.; Chang, K. Y.; Chen, Y. P.; Chen, L. Y. Dual inhibition effect of reline deep eutectic solvent on methane hydrate nucleation and formation. *Fuel* **2022**, *328*, 125376.
(22) Pandey, G.; Veluswamy, H. P.; Sangwai, J.; Linga, P. Morphology study of mixed methane−tetrahydrofuran hydrates with and without the presence of salt. *Energy Fuels* **2019**, *33* (6), 4865−4876.
(23) Yu, Y. S.; Sun, W. Z.; Chen, C.; Li, X. S.; Chen, Z. Y. Kinetics studies of methane hydrate formation and dissociation in the presence of cyclopentane. *Fuel* **2024**, *356*, 129651.
(24) Huang, C.; Lin, R.; Lu, C.; Yu, X.; Yang, Z.; Wu, C.; Li, J.; Wang, Y. Effects of gas to water ratio and nano-Cu dosage on CH4 hydrate growth: A combined molecular simulation and experimental study. *Fuel* **2024**, *357*, 129663.
(25) Omran, A.; Nesterenko, N.; Valtchev, V. Driving sustainable energy storage: A multi-scale investigation of methane hydrate formation with green promoters and innovative reactor design. *J. Energy Storage* **2024**, *75*, 109653.
(26) Mohammadi, A.; Manteghian, M.; Mohammadi, A. H.; Jahangiri, A. Induction time, storage capacity, rate of methane hydrate formation in the presence of SDS and silver nanoparticles. *Chem. Eng. Commun.* **2017**, *24* (12), 1420−1427.
(27) Ngema, P. T.; Petticrew, C.; Naidoo, P.; Mohammadi, A. H.; Ramjugernath, D. Experimental measurements and thermodynamic modelling of the dissociation conditions of clathrate hydrates for (refrigerant + NaCl + water) systems. *J. Chem. Eng. Data* **2014**, *59*, 466−475.
(28) Ndlovu. Carbon dioxide encapsulation in methane hydrates. Ph.D. thesis, Department of Chemical Engineering. School of Agriculture, Science and Engineering. University of KwaZulu Natal, Durban, South Africa, 2022.
(29) Babaee, S.; Hashemi, H.; Mohammadi, A. H.; Naidoo, P.; Ramjugernath, D. Kinetic study of hydrate formation for argon + TBAB + SDS aqueous solution system. *J. Chem. Thermodyn.* **2018**, *116*, 121−129.
(30) Fakir, T.; Babaee, S.; Naidoo, P. Application of gas hydrate for the treatment of Vinasse: Phase Equilibrium and Kinetic investigations. *J. Chem. Eng. Data* **2021**, *66* (1), 504−514.
(31) Klauda, J. B.; Sandler, S. I. A fugacity model for gas hydrate phase equilibria. *Ind. Eng. Chem.* **2000**, *39*, 3377−3386.
(32) Valderrama, J. O. A generalized Patel-Teja Equation of State for polar and nonpolar Fluids and their Mixtures. *J. Chem. Eng. Jpn.* **1990**, *23*, 87−91.
(33) Demirbas, A. Methane hydrates as a potential energy resource: Part 2- Methane production processes from gas hydrates. *Energy Convers. Manag.* **2010**, *51*, 1562−1571.
(34) Chatti, I.; Delahaye, A.; Fournaison, L.; Petite, J.-P. Benefits, and drawbacks of clathrate hydrates: A review of their areas of interest. *Energy Convers. Manag.* **2005**, *46*, 1333−1343.

https://doi.org/10.1021/acs.energyfuels.3c04584
Energy Fuels 2024, 38, 4480−4491